Build Simul
https://doi.org/10.1007/s12273-020-0624-3

Numerical simulation of heat transfer in a roof assembly with reflective insulation and radiant barrier

Muhamad Zahin Mohd Ashhar, Chin Haw Lim (✉)

Solar Energy Research Institute (SERI), National University of Malaysia, 43600 Bangi, Selangor, Malaysia

Abstract

The increasing demand of reducing energy consumption in buildings has led to the implementation of insulation material in roof assemblies to reduce heat gain through the roof. This paper investigates the thermal performance of reflective insulation and radiant barrier systems in a gable roof assembly by using computational fluid dynamics (CFD) simulation. In the first part of the paper, the experimental measurements using test huts under actual outdoor environment were detailed. The CFD simulation was then conducted and the results obtained from the simulation were validated against the experimental measurements. In the second part paper, the validated CFD model was then used to evaluate the reduction of heat flux transmission through the roof and the thermal resistance (RSI value) of the roof assemblies for various roof configurations, which are the thickness of reflective air space, the roof pitch and the roof material. The study showed that increasing the reflective air space thickness from 25 mm to 100 mm has increased the total RSI by 26% for both roof pitch of 30° and 45°. Besides that, increasing the roof pitch of the roof from 30° to 45° showed that biggest impact on the thermal performance of the roof, as the RSI value increases by 30%. In terms of roof tiles material, only small difference was observed in terms of thermal resistivity when switching the roof tiles material between clay tiles and concrete tiles.

Keywords

reflective insulation,
radiant barrier,
CFD,
roof insulation,
thermal performance

Article History

Received: 01 August 2019
Revised: 14 January 2020
Accepted: 15 February 2020

1 Introduction

Malaysia's climate is hot and humid, with high average temperatures of 31.0 °C–33.0 °C and high relative humidity throughout the year. The daily annual average solar irradiations ranging between 4.21 kWh/m^2 and 5.56 kWh/m^2 (Sarawak Energy 2017). A large percentage of the incoming heat energy is absorbed by the exposed roof surfaces and much of this energy is transmitted into the building. Although every component of a house contributes to heat gain and heat loss of a house, the roof is the component that contributes to the high-temperature gain and loss (Hernández-Pérez et al. 2014). In hot climates, the roof is responsible for the high cooling load of buildings (Nahare et al. 2003). By implementing a suitable insulation system in a roof assembly, heat flow into a building can be reduced up to 45% (Medina 2012). Bulk insulation materials are commonly used for thermal insulation. However, in a tropical climate where radiative heat energy flows downwards predominate, radiant barrier and reflective insulation systems are the effective thermal insulation options to be implemented in a roof assembly (Teh et al. 2017). The heat transfer mechanism in a residential gable roof is illustrated in Figure 1.

1.1 Background of study

To preserve the indoor thermal comfort in a building, the heat energy due to solar radiation through the roof needs to be minimized. As the cost of energy increases, efficient use of energy becomes more urgent and the dependency on using air-conditioning for indoor cooling needs to be reduced. Ideally, buildings should be designed and constructed to have all the outstanding features of energy efficiency, thermal comfort, affordable and be ecologically friendly. One of the strategies is to implement a thermal insulation material in the roof assembly.

The purpose of thermal insulation materials is to slow down the transmission of heat energy into or out of the building. As illustrated in Figure 2, thermal insulation

E-mail: chinhaw.lim@ukm.edu.my

List of symbols

c	specific heat capacity (J/(K·kg))
E	emissivity
g_i	gravitational acceleration component along the i-th coordinate direction (m/s^2)
h	thermal enthalpy (J)
N	number of fitted points
Q_H	heat source of sink per unit volume (W)
q_i	diffusing heat flux (W/m^2)
S_i	mass-distributed external force per unit mass
t	thickness of reflective air space (mm)
u	fluid velocity (m/s)
τ_{ij}	viscous shear stress tensor (Pa)
λ	thermal conductivity (W/m·K)
ρ	density (kg/m^3)

Abbreviations

3D	three dimensional
CFD	computational fluid dynamics
MAPE	mean absolute percentage error
RSI	thermal resistance
SERI	Solar Energy Research Institute
UKM	National University of Malaysia

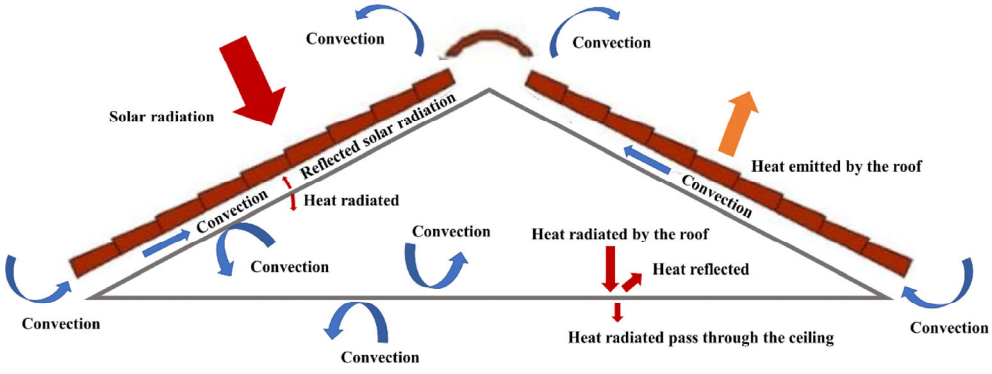

Fig. 1 Heat transfer mechanism in a gable roof

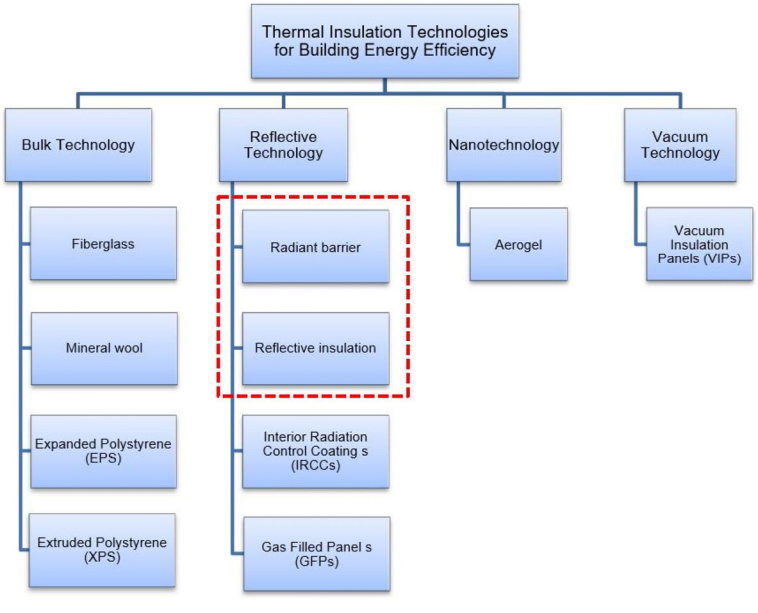

Fig. 2 Insulation materials classification (Lee et al. 2016)

technologies used in buildings are predominantly bulk and reflective technologies. The technologies that work on reducing radiative heat transfer through building components are categorized as reflective insulation and radiant barrier systems. Both systems utilize materials that have low emissivity characteristics to decrease the transmission of

heat gain through one or more enclosed air spaces (RIMA 2002). These systems are dependent on air, which has low thermal conductivity characteristics to reduce heat transfer across the systems. The reflective insulation system is defined by utilizing a material with low emissivity parallel to an enclosed air space. A reflective insulation system contains air space thickness up to 0.25 m perpendicular to the direction of heat transmission. The thermal resistance of the reflective insulation system is the product of the reduction of heat transfer through the enclosed air space. Besides that, the thermal resistance of the reflective insulation system depends on the inclination as it would affect the rate of convective heat transfer inside the air space. As opposed to reflective insulation systems, radiant barrier systems have larger air space which is usually thicker than 0.5 m. The ability of a radiant barrier system to perform depends on the direction of heat transmission, which would vary in different seasons (Yarbrough 2010).

In the reflective insulation system, reflective foil (commonly aluminium foil) is installed under the roof tiles separated by battens, creating an air space between the roof tiles and the reflective foil. Although the definition of reflective insulation system says that the reflective foil must be facing an enclosed air space, it is merely impossible to make the air space between roof tiles and reflective foil as airtight. The roof tiles' linkages provide air movement between the air space and the outside, which allows air ventilation to be a contributing factor in the system. On the other hand, the reflective foil facing the vented attic space makes up the radiant barrier system. The effectiveness of a radiant barrier system is hugely affected by the attic ventilation in the attic space. These two systems can be coupled in a roof assembly and the implementation of these two systems is illustrated in Figure 3.

1.2 Malaysian Standard (MS 1525)

The motivation of this study rose from the latest insertion of MS 1525 to Uniform Building By-Law (UBBL) Section 38A-(2), which requires residential and non-residential buildings to obtain authority approval in the achievable thermal transmittance (*U*-value). According to UBBL Section 38A-(2), the roof of all buildings (residential and non-residential) shall not have a U-value greater than 0.4 W/(m^2·K) (RSI value of 2.5 m^2·K/W) for lightweight roof (under 50 kg/m^2) and 0.6 W/(m^2·K) (RSI value of 1.67 m^2·K/W) for heavyweight roof (above 50 kg/m^2) unless provided with other shading and cooling means (Department of Standards Malaysia 2014). The implementation of this regulation is still unclear, and the authority has yet to have a method to calculate the *U*-value or RSI value of the entire roof.

1.3 Previous work

Numerous research works have been carried out in analyzing the parameters that affect the performance of reflective insulation and radiant barrier systems. The influence of emissivity properties of the insulation material on the thermal performance of a pitched roof assembly has been investigated previously (Roels and Deurinck 2011; Yarbrough et al. 2016). It is proven that lower emissivity characteristics of insulation material would result in a higher reduction of heat penetration into the attic space. The thermal performance of low emissivity assembly was reported by Saber (2013). It was stated that low emissivity material contributes to a higher thermal resistivity of an assembly. Furthermore, the use of aluminum foil as the low emissivity insulation material in a roof assembly was investigated previously

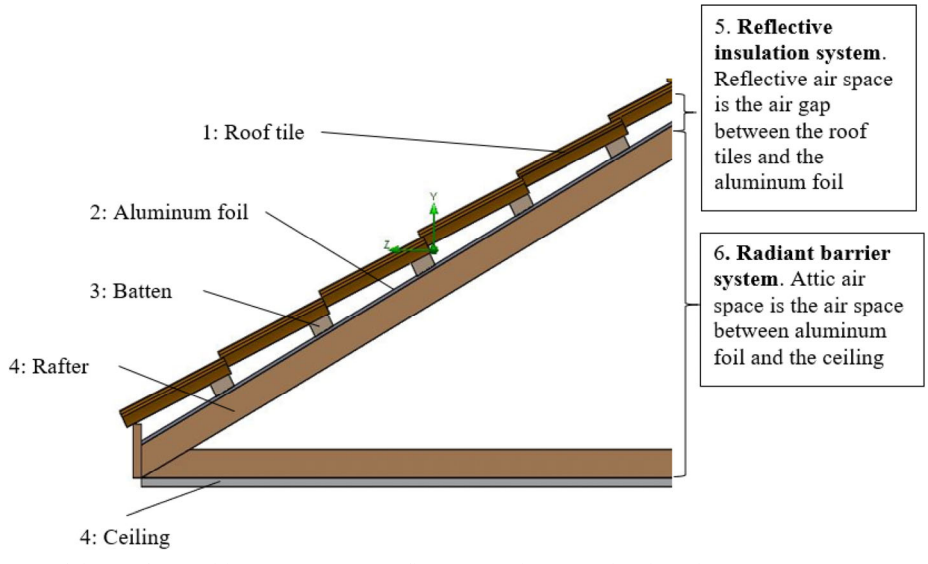

Fig. 3 The cross section of the roof assembly incorporating reflective insulation and radiant barrier systems

(Dos Santos and Mendes 2015). The researchers developed a mathematical model to analyze the reduction of heat flux when aluminum foil is used as the insulation material in a roof assembly. The use of aluminum foil which has a low emissivity characteristic as the insulation layer under the roof reduces 40% of the heat flux of the internal roof surface.

The thickness of reflective air space is one of the significant configurations affecting the performance of a reflective insulation system. Ample amount of airspace is required to minimize the radiant heat transfer through the reflective air space. The low thermal conductivity of the air is responsible in reducing heat radiation transmission through the air space (Troppova et al. 2018). Although the reflective air space in the reflective insulation system is meant to be airtight, a certain degree of air flow into the reflective air space is inevitable due air permeability of the roof tiles (Fantucci and Serra 2019). On the bright side, it was found that the air ventilation gives a massive impact in reducing solar heat penetration across the roof system and consequently improves indoor thermal comfort (Dimoudi et al. 2006). The combined effect of insulation material and the air ventilation within the ventilated air space caused by the convective heat transfer removes heat as the hot air flow from the ridge and escapes through the ridge (Roels and Deurinck 2011). Larger air layer thickness is good to enhance the rate of air flow and reduce the roof tiles temperature (Li et al. 2016). Besides that, promoting a higher air flow rate in the attic roof space will increase the percentage of heat flux reduction in a roof assembly with a radiant barrier system (Miranville et al. 2012; Gagliano et al. 2012).

Several methods of researches have been conducted on the installation of a radiant barrier system in attic system to reduce the inward heat transmission through the ceiling. Medina (2000) conducted both computational simulation and experimental measurements to study the use of radiant barrier system in the attic space of a residential house. The percentage of heat flux reduction through the roof was presented between 25% and 42%, and the results also presented that the ability of the radiant barrier in reducing radiative heat transfer was poorer when stronger attic insulation was used. The study was further extended to evaluate the radiant barrier system's capability in different climates in the United States (Medina and Young 2006). The study was conducted by computer simulation for a radiant barrier in a vented triangular attic space. The results suggested that the percentage of heat penetration reduction through the ceiling is different for different climates due to the different direction of heat flow. Hence, the ability of the attic radiant barrier to reduce heat transmission is dependent on the location of the building. Certain environmental factors such as the local ambient air temperature, cloudiness, humidity, and altitude have a major influence on the performance of the radiant barrier system. The percentage of heat flux through the ceiling varied from 36.8% in the Tropical Savanna climate to 2.3% in the Mediterranean climate. Soubdhan et al. (2005) researched on the use of different insulation materials on the heat transfer reduction in a building roof. Four test cells were built for four insulation configurations which are; polystyrene, radiant barrier, fiberglass and no insulation as the reference cell. The results showed that the radiant barrier was able to reduce the heat flux transmission between 33% and 37% as compared to the non-insulated reference cell. Their results also stated that a layer of air ventilation is necessary to provide the escape path for the reflected heat flux. From their research, the researchers concluded that the radiant barrier was the best type of insulation material when ventilation occurs in the air space. Miranville et al. (2012) conducted a field test to study the use of multi-reflective radiant barrier (MRRB) applied on a roof. To study the effect of air ventilation, the top air space layer was mechanically ventilated. From their research, it was found that the MRRB successfully reduced a huge amount of heat flux through the roof. Even more when the air space is ventilated. Higher air flow rate results in higher heat flux reduction and higher overall thermal resistance of roof assembly. Recently, Fantucci and Serra (2019) researched on the comparison between reflective insulation in the form of aluminum foil and low-emissivity paint applied below the roof tiles in a roof system by in-field measurement. Their results showed that the reflective insulation was able to perform better than the low-emissivity paint. The reflective insulation showed a reduction of heat flux during summer between 10% and 53% and a maximum reduction of the indoor temperature by 1.2 °C.

Another parameter that has been studied is the effect of varying the roof pitch on the thermal performance of a roof assembly. The previous study on the impact of roof pitch on the cooling load of gable-roof residential buildings was previously researched by Wang et al. (2012). The research was done by implementing a 2D CFD model, simulating turbulent air flow in the attic space for various roof pitches. Their research found that increasing the roof pitch from 3/12 to 8/12 resulted in a reduction of cooling load by 9%. They also suggested that changing the roof pitch alone has a small effect on the reduction of attics cooling load. Their research, however, is only focused on the roof attic space and neglected the influence of other roof structures which may have a bigger effect on the thermal performance of the roof assembly. The effect of changing the roof slope on the exhausted heat was previously studied and it was found that when the roof slope was increased to 55°, an airflow was developed and causes the airflow velocity and the temperature difference increased. Steeper roof slope resulted in a higher

amount of exhausted heat because of the buoyancy force (Lee et al. 2009).

In the studies presented in the literature, the parameters that have an effect on the thermal performance of a radiant barrier system such as the emissivity of reflective foil, the reflective air space thickness, roof pitch and the inclination angle of enclosed air space have been presented. However, the combination of reflective insulation and radiant barrier system in a roof assembly is yet to be explored. The thickness and inclination angle of reflective air space may cause discrepancies on the air movement inside the air space which would affect the thermal resistivity of the roof assembly. Furthermore, varying the roof pitch may have an effect on the heat transfer via heat convection through the attic space, and the thermal performance of this parameter has been barely studied. Besides that, there is no previous work that studied on measuring the thermal conductivity (U-value) or thermal resistivity (RSI value) of the entire insulated roof assembly. Therefore, this research aims to study the thermal performance of an entire insulated roof assembly for various roof configurations, which are the reflective air space thickness, roof pitch and the roof tile material. The thermal performance of the thermal insulation systems is evaluated by investigating the reduction of heat flux across the roof assembly, and by calculating the thermal resistance (RSI value) of the entire roof assembly. Based on the literature review, there's still no research conducted to study the thermal performance of thermal insulated roof in the tropical climate of Malaysia. Hence, this research aims to fill in the research gap.

2 Experimental measurements

The experimental measurement of this research was done by a researcher from Solar Energy Research Institute (SERI) of the National University of Malaysia (UKM) (Teh et al. 2017). The experimental measurement was done by constructing three identical test huts in Melaka, Malaysia as shown in Figure 4. The roof assemblies of the test huts are gable roof with a pitch of 30°. The reflective foil was installed under the roof tiles, laid on the rafters and separated by battens, creating the reflective air space. The data collection was done over a period of 12 months from May 2016 to April 2016 for various configurations.

2.1 Data acquisition monitoring system

In each test hut, a total of 12 Type-K thermocouples with a precision of ±1 °C were installed in three different positions which were below the roof tiles, below the reflective foil and on top of the ceiling. This is to measure and monitor the surface temperature of the materials. Besides that, a heat flux transducer was attached on top of the ceiling to measure the heat flux across the ceiling as shown in Figure 5.

2.2 Calculation of RSI from transient data

The thermal performance of the insulated roof assembly was measured by calculating the thermal resistance, RSI value of the entire roof assembly. By using the measured surface temperature and heat flux values obtained from the thermocouples and HFTs respectively, the RSI value of the roof assembly can be derived using the following formula:

$$\mathrm{RSI}_{\mathrm{Total}} = \mathrm{RSI}_A + \mathrm{RSI}_B \tag{1}$$

$$\mathrm{RSI}_{\mathrm{Total}} = \frac{T_1 - T_2}{q_A} + \frac{T_2 - T_3}{q_B} \tag{2}$$

where,
RSI_A is the RSI value of the reflective air space;
RSI_B is the RSI value of the attic air space;

Fig. 4 Test huts construction in Melaka

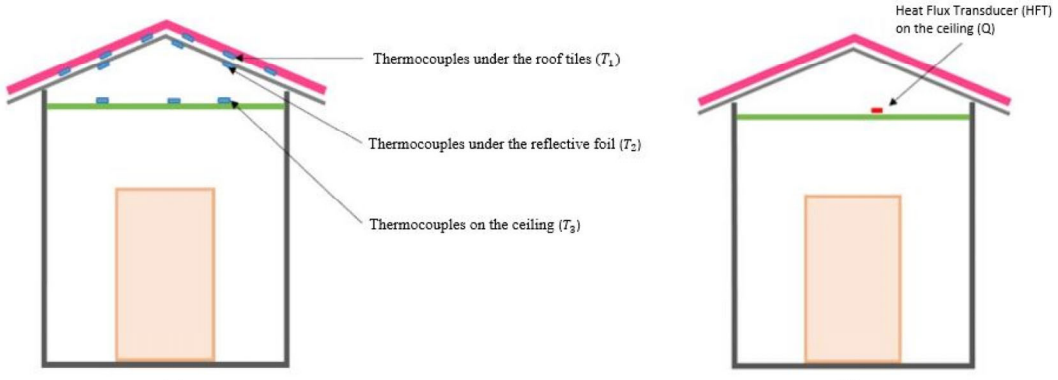

Fig. 5 (a) position of thermocouples in the roof assembly; (b) position of heat flux transducer (HFT) on top of the ceiling

RSI_{Total} is the RSI of the entire roof assembly;
T_1 is the average surface temperature of roof tiles;
T_2 is the average surface temperature of reflective foil;
T_3 is the average surface temperature of the ceiling;
q_A is the heat flux across the reflective air space;
q_B is the heat flux across the ceiling.

Table 1 shows the RSI values result of the 4 configurations of roof assembly that have been conducted through experimental setup.

Table 1 The RSI values obtained from the experimental measurements (Teh et al. 2017)

Case	Roof type	Air space thickness (mm)	Roof pitch (°)	RSI value (m^2·K/W) from experimental measurement
1	Clay tiles	25	30	2.40
2	Concrete tiles	25	30	2.15
3	Concrete tiles	25	30	2.26
4	Concrete tiles	25	30	2.37

3 CFD model

In this research, FloEFD—a CFD package tool was used to solve the 3D steady-state model condition. All three modes of heat transfer (conduction, convection, and radiation) were considered in the simulation. Solar radiation was directed towards the roof tiles, to mimic the actual condition of a typical hot and humid Malaysian weather. FloEFD can predict both laminar and turbulent flows. To predict the laminar-turbulent flows, the conservation of energy, mass, and momentum (Favre-averaged Navier-Stokes) equations were employed. To solve the system of equations, FloEFD uses *the k-ε model* to employ transport equations for the turbulent kinetic energy and its dissirateon rate. Unlike other traditional CFD solver, FloEFD uses only one system of equations to solve both laminar and turbulent flows. The three-dimensional equations for the conservation laws of mass, angular, momentum, and energy in the Cartesian coordinate system can be written in the conservation form as follows:

$$\frac{\partial \rho}{\partial t} + \frac{\partial}{\partial y}(\rho u_i) = 0 \tag{3}$$

$$\frac{\partial \rho u_i}{\partial t} + \frac{\partial}{\partial x_j}(\rho u_i u_j) + \frac{\partial p}{\partial x_i} = \frac{\partial}{\partial x_j}(\tau_{ij} + \tau_{ij}^R) + S_i, \quad i = 1,2,3 \tag{4}$$

$$\frac{\partial \rho H}{\partial t} + \frac{\partial \rho u_i H}{\partial x_i} = \frac{\partial}{\partial x_i}\left(u_j(\tau_{ij} + \tau_{ij}^R) + q_i\right) + \frac{\partial p}{\partial t} - \tau_{ij}^R \frac{\partial \rho u_i}{\partial x_j} + \rho\varepsilon + S_i u_i + Q_H \tag{5}$$

$$H = h + \frac{u^2}{2} \tag{6}$$

where u is the fluid velocity, ρ is the density, S_i is a mass-distributed external force per unit mass due to a porous media resistance (S_i^{porous}), a buoyancy ($S_i^{gravity} = -\rho g_i$, where g_i is the gravitational acceleration component along the i-th coordinate direction), and the coordinate system's rotation ($S_i^{rotation}$), i.e., $S_i = S_i^{porous} + S_i^{gravity} + S_i^{rotation}$, h is the thermal enthalpy, Q_H is a heat source of sink per unit volume, τ_{ij} is the viscous shear stress tensor, R is the distance from a point to rotation axis in rotation reference, q_i is the diffusing heat flux.

Turbulent kinetic energy and dissipation are described by two additional transport equations which are,

$$\frac{\partial \rho k}{\partial t} + \frac{\partial}{\partial x_i}(\rho u_i k) = \frac{\partial}{\partial x_i}\left(\left(\mu + \frac{\mu_t}{\sigma_k}\right)\frac{\partial k}{\partial x_i}\right) + S_k \tag{7}$$

$$\frac{\partial \rho \varepsilon}{\partial t} + \frac{\partial}{\partial x_i}(\rho u_i \varepsilon) = \frac{\partial}{\partial x_i}\left(\left(\mu + \frac{\mu_t}{\sigma_\varepsilon}\right)\frac{\partial \varepsilon}{\partial x_i}\right) + S_\varepsilon \tag{8}$$

where S_k and S_ε are defined as

$$S_k = \tau_{ij}^R \frac{\partial u_i}{\partial x_j} - \rho\varepsilon + \mu_t P_B \tag{9}$$

$$S_\varepsilon = C_{\varepsilon 1}\frac{\varepsilon}{k}(f_1 \tau_{ij}^R \frac{\partial u_i}{\partial x_j} + \mu_t C_B P_B) - C_{\varepsilon 2} f_2 \frac{\rho\varepsilon^2}{k} \tag{10}$$

Here P_B represents the turbulent generation due to buoyancy forces and can be written as

$$P_B = -\frac{g_i}{\sigma_B}\frac{1}{\rho}\frac{\partial \rho}{\partial x_i} \tag{11}$$

where g_i is the component of gravitational acceleration in direction x_i, the constant $\sigma_B = 0.9$, and constant $C_B = 1$. The values of constants taken from FloEFD technical reference are $C_\mu = 0.09$, $C_{\varepsilon 1} = 1.44$, $C_{\varepsilon 2} = 1.92$, $\sigma_k = 1$, $\sigma_\varepsilon = 1.3$ (Mentor Graphics Cooperation 2017).

3.1 Roof configuration

In the CFD model, the heat transfer through the gable roof assembly was studied independently, as the influence of other building structures was not included. The modelled roof structures replicate the roof of the test huts as detailed in the experimental measurements. In addition, a roof pitch of 45° was also modelled to investigate the effect of varying the roof pitch on the thermal performance of the insulated roof assembly. The geometries of the analysed gable roof assemblies are shown in Figure 6.

Figure 7 shows the main components of the investigated gable roof assembly incorporating reflective insulation and radiant barrier systems. The assembly configuration is the same for both 30° roof pitch and 45° roof pitch. The total length, width, and height of the roof assemblies are 4.2 m × 3.3 m × 1.7 m and 3.5 m × 3.3 m × 2.1 m for the roof pitch of 30° and 45° respectively which can be seen in Figure 6. The roof pitch of 45° has taller height and shorter length as the pitch was increased while keeping the same total surface area of roof tiles. The cross-section view of the roof assembly can be referred to in Figure 3.

Table 2 details the investigated roof configurations done in this research where reflective air space thickness of 25 mm, 50 mm, 75 mm and 100 mm for roof pitch of 30° and 45° are studied. Reflective air space thickness less than 25 mm and 100 mm are not studied in this research. Similarly, roof pitches other than 30° and 45° are also not considered in this research.

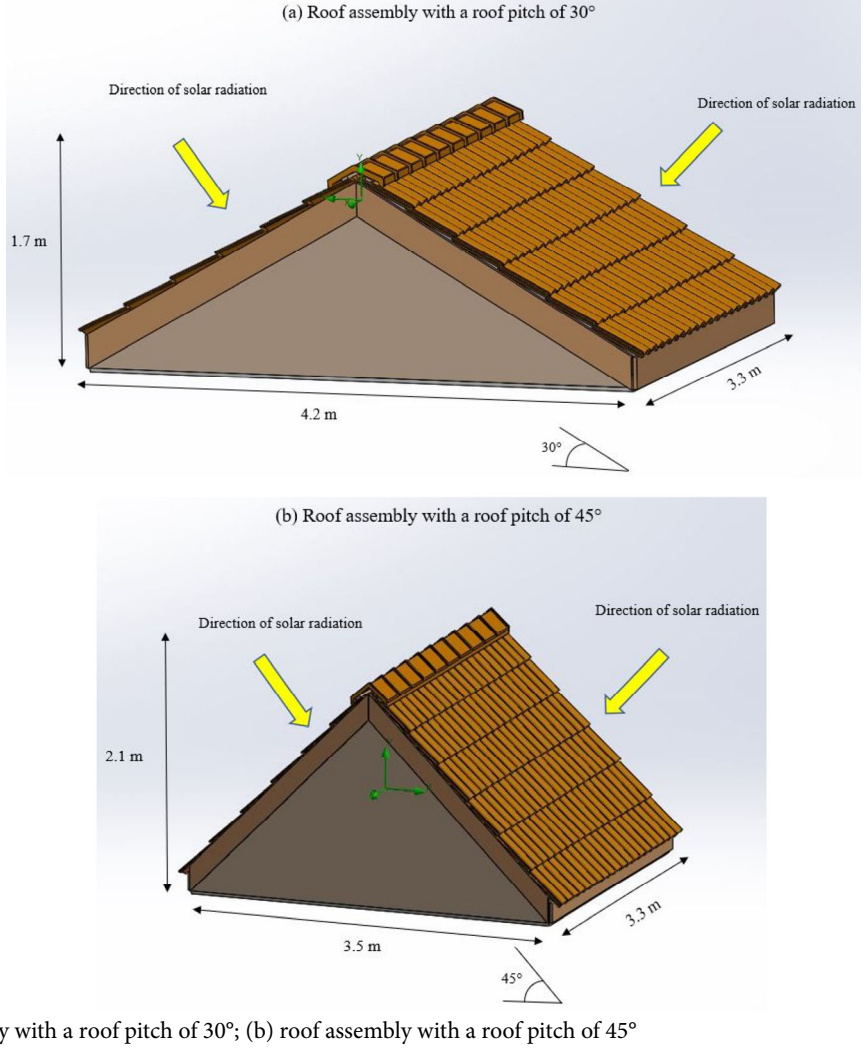

Fig. 6 (a) roof assembly with a roof pitch of 30°; (b) roof assembly with a roof pitch of 45°

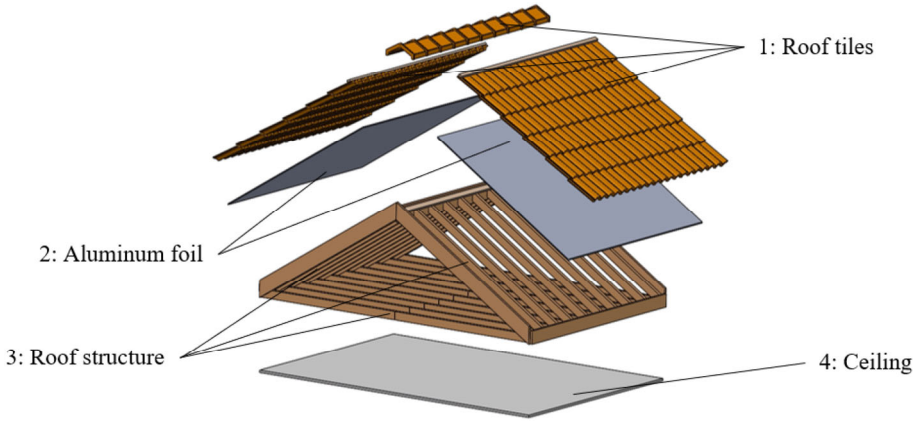

Fig. 7 Exploded view of the typical gable roof assembly with radiant barrier system

Table 2 The investigated configurations using CFD simulation

Roof type	Reflective air space thickness (mm)	Roof pitch (°)
Clay tile	25, 50, 75, and 100	30 and 45
Concrete tile	25, 50, 75, and 100	30 and 45

3.2 Boundary conditions

The materials used in the CFD simulation are:

- Air as the fluid domain
- Clay tiles or concrete tiles as roof tiles
- Aluminium foil as the reflective insulation material
- Wood as the rafters, battens, and ridge
- Gypsum board as the ceiling

The properties of the materials obtained from FloEFD database that were used in the simulation are listed in Table 3.

As the CFD simulation aims to simulate the heat transfer through the gable roof assembly at an outdoor environment, external type analysis was used. The CFD computational conditions used to simulate Malaysia outdoor environment are listed in Table 4.

The mesh quality affects the sensitivity and accuracy of the results when compared to the empirical measurement results. Hence, to achieve the accurate analysis of the roof assemblies, a finer mesh was employed in regions with more geometry complexity such as the roof tiles. Finer mesh was also used on the materials that require higher sensitivity for accurate results such as the aluminum foil and the ceiling. Coarser mesh was used on the other roof structures such as the rafters, ridge, and in all other regions. Finer mesh was also used in corners and small edges of the roof structures as seen in Figure 8. One of the features of FloEFD is to employ local mesh refinement on the intended components. This feature was used on the roof tiles, the aluminum foil, and the ceiling, with the highest level of refinement was employed on the roof tiles due to the geometric complexity.

Table 3 List of material properties used in the simulation

Material	Emissivity ε	Thermal conductivity λ (W/(m·K))	Specific heat capacity c (J/(K·kg))	Density ρ (kg/m^3)
Clay tiles	0.9	0.83	800	1900
Concrete tiles	0.9	1.10	837	2100
Gypsum board	0.85	0.16	840	950
Wood	0.9	0.14	1200	650
Aluminium foil	0.03	0.896	167	2689

Table 4 The computational condition used in the CFD simulation

CFD Computational condition	Value
Ambient temperature	33 °C
Heat radiation directed towards the roof tiles	600 W/m² – 1000 W/m²
Atmospheric pressure	101.3 kPa
Air velocity	0.5 m/s
Relative humidity	60%
Cloudiness index	0.3

This results in tetrahedral mesh cells on the roof tiles which is a better mesh type in capturing results in complex geometry. The number of total cells used in the simulations was over 200,000 fluid cells and solid cells, and the results converge after over 200 iterations.

3.3 RSI values calculation from CFD simulation

This research utilizes the same formula to RSI values of the roof assembly as previously used by Teh et al. (2017) which was detailed in Eq. (2). From the CFD simulation, few readings are collected from the simulation to make full use of Eq. (2). The data collected from the simulation are (Figure 9):

(1) The average surface temperature of the roof, T_1.

(2) The average surface temperature of the radiant barrier, T_2.

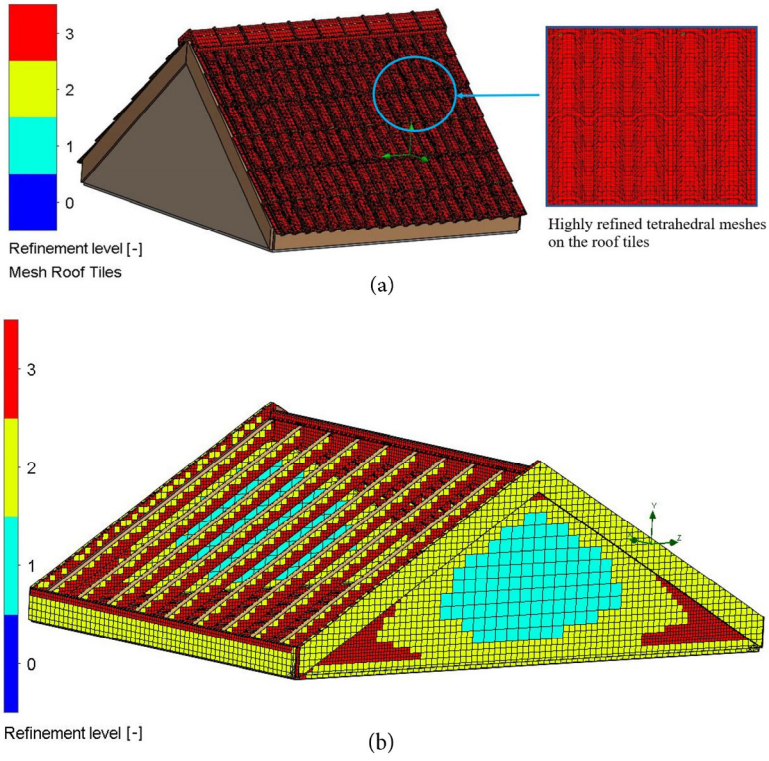

Fig. 8 (a) tetrahedral meshes type on the roof tiles; (b) hexahedral mesh type on the roof structure

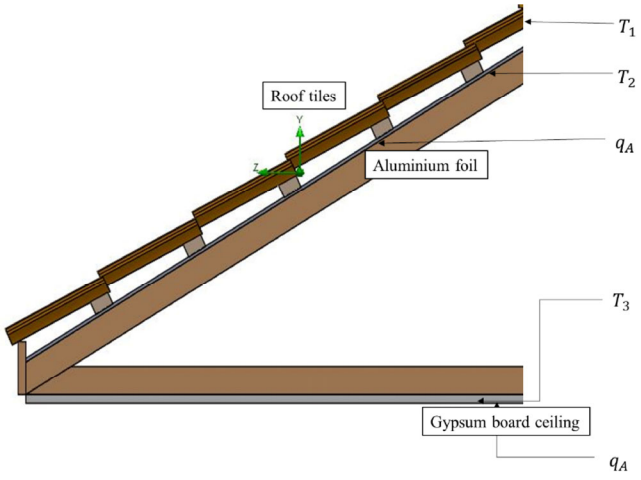

Fig. 9 The readings taken from the CFD simulation

(3) The average surface temperature of the top of the ceiling, T_3.
(4) The average heat flux across the reflective air space, q_A.
(5) The average heat flux across the attic, q_B.

By using the readings taken from the CFD simulation, RSI_A and RSI_B values were calculated using the following formula:

$$RSI_A = \frac{T_1 - T_2}{q_A} \tag{12}$$

$$RSI_B = \frac{T_2 - T_3}{q_B} \tag{13}$$

As described earlier, RSI_A represents the RSI value for the reflective air space which is between the roof tiles and the aluminium foil and RSI_B represents the RSI value for the attic space which is between the aluminium foil and the ceiling. Hence, the total RSI value is the summation of RSI_A and RSI_B as shown in Eq. (1).

4 Results and discussion

4.1 CFD results validation against experimental measurements

To ensure that the results obtained by CFD simulation are acceptable, the CFD results must first be validated against some of the empirical results obtained by field test conducted by Teh et al. (2017). Due to limitations in conducting the field experiment, the RSI values obtained from CFD simulation and experimental measurements can only be compared against available data which are shown in Table 5.

Figure 10 shows a comparison between the predicted RSI values using FloEFD and the measured RSI values for various configuration in different phases. As shown in Figure 10, the predicted RSI values obtained from CFD simulation for all configurations are in good agreement with the measured RSI values as the prediced RSI values are within the ± 95% confidence band. Furthermore, the mean absolute percentage error between the CFD simulation and

Table 5 Cases used for CFD results validation against experimental measurements

Case	Roof type	Air space thickness (mm)	Roof pitch (°)	RSI value (m^2·K/W) from experimental measurement (Teh et al. 2017)	Predicted RSI value (m^2·K/W) from CFD simulation (this paper)	Percentage error (%)
1	Clay tiles	25	30	2.40	2.37	1.25
2	Concrete tiles	25	30	2.15	2.33	8.37
3	Concrete tiles	25	30	2.26	2.33	3.10
4	Concrete tiles	25	30	2.37	2.33	1.69
Mean absolute percentage error						**3.60**

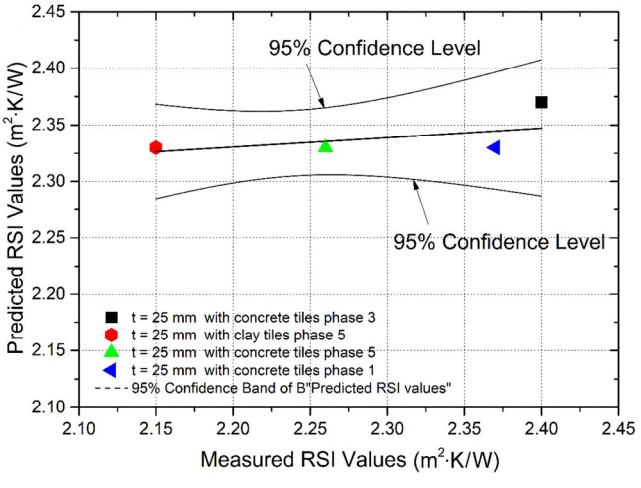

Fig. 10 Comparison of the predicted RSI values with the measured RSI values

experimental measurements is 3.60%, which is acceptable. Once the results are validated, then it can be said that the 3D model, assumptions, and boundary conditions are able to predict accurate values with high confidence. From here, the exact same 3D model, along with the assumptions and boundary conditions will be used to investigate the other roof configurations.

4.2 Heat flux penetration through the gable roof assemblies

In this section, the heat flux penetration will be analyzed in two parts: (a) heat flux penetration through the reflective air space and (b) heat flux penetration through the attic. The percentage of heat flux reduction will also be presented for all roof configurations.

Figure 11 illustrates the heat flux penetration through the reflective air space area of the roof assemblies. It can be noted that the heat flux penetration through the reflective air space decreases exponentially as the air space thickness increased from 25 mm to 100 mm. This is because the air ventilation inside the reflective air space area increases as the thickness of reflective air space increase from 25 mm to 100 mm. This causes the rate of hot air flow from the eaves to ridge increases (Roels and Deurinck 2011). Stronger air flow rate inside the reflective air space area increases the convective heat transfer. Therefore, heat loss through convective heat transfer increases and the heat flux penetration into the roof assembly due to solar radiation decreases. However, when a smaller thickness of reflective air space is used, the drag force that causes friction to become larger and contributes to restricting the air movement and hence reduces convective heat transfer (Alzwayi and Paul 2014). As a result, the heat radiation traps inside the reflective air space and transmits into attic. As the reflective air space is further inclined to 45° from 30°, the heat flux transmitted through the reflective air space area is much lesser and this phenomenon agrees with an empirical measurement done by Tong and Li (2014).

Figure 12 shows the heat flux penetration through the attic space of the roof assemblies for a gable roof pitch of 30° and 45°. The heat flux penetration through the attic space for a gable roof pitch of 45° was consistently lower than roof pitch of 30° for both types of roof tile materials. Hence, it can be argued that the pitch of the attic space contributes to a higher impact in the reduction of heat flux penetration through the gable roof assembly. While

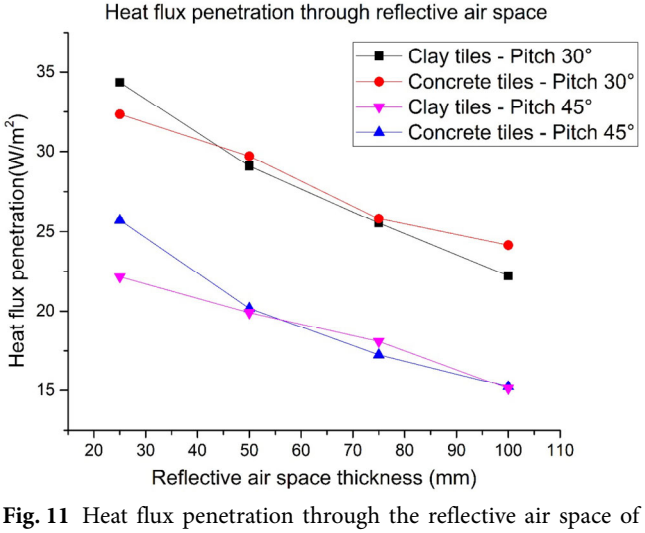

Fig. 11 Heat flux penetration through the reflective air space of the roof assemblies

increasing the thickness reflective air space from 25 mm to 100 mm have a bigger effect on reducing the heat flux transmission through the attic air space for a gable roof pitch of 30°, a much lesser impact can be noted for a gable roof pitch of 45°. One possible reason is that the rate of convective heat transfer inside the attic space area overshadows the impact of convective heat transfer inside the reflective air space.

Figure 13 shows the percentage of heat flux reduction at the ceiling when an aluminum foil was installed in the roof assembly. The percentage of heat flux reduction varies between 84% and 87% for a gable roof pitch of 45° whereas the percentage of heat flux reduction was between 79% and 88% for a gable roof pitch of 30° for reflective air space between 25 mm and 100 mm. It can be noted that the roof assemblies show a logarithmic increment of heat flux reduction as the reflective air space was increased from

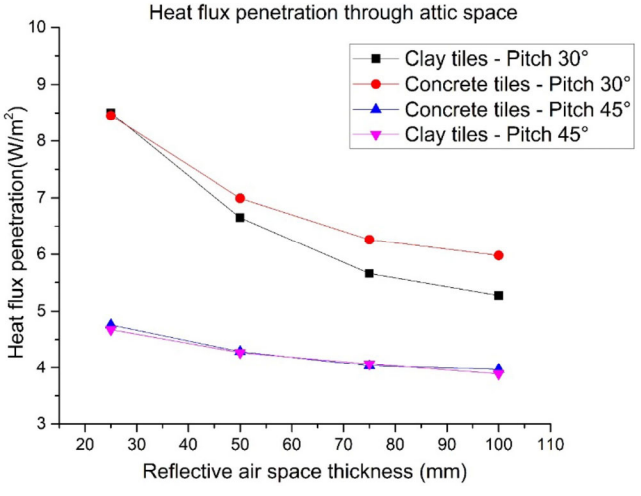

Fig. 12 Heat flux penetration through the attic space of the roof assemblies

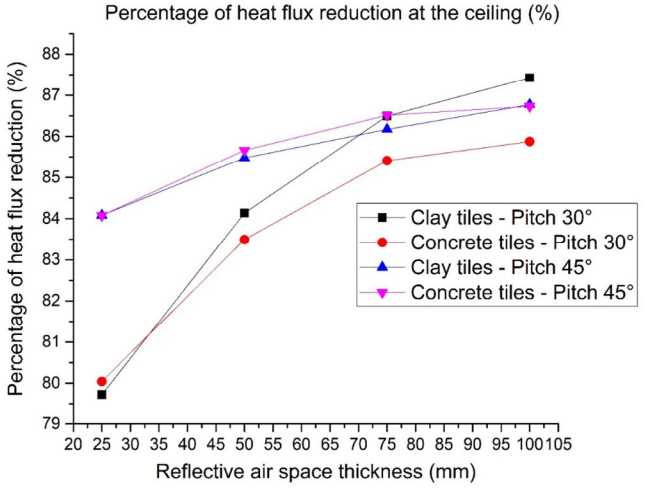

Fig. 13 Percentage of heat flux reduction at the ceiling of the roof assemblies

25 mm to 100 mm. At reflective air space thickness of 25 mm, gable roof pitch of 45° shows a higher percentage of heat flux reduction compared to a gable roof pitch of 30°. However, as the reflective air space was increased from 25 mm to 100 mm, the percentage of heat flux reduction converges to a value between 85% and 88%. This can be explained by the fact that as the reflective air space was increased from 25 mm to 100 mm, the temperature gradient between roof surfaces (i.e. roof tiles and the ceiling) get smaller and hence buoyancy force increases at a lower rate. Thus, the rate of airflow and convective heat transfer increase at a slower rate despite having a thicker reflective air space (Tong and Li 2014).

4.3 Predicted RSI values from CFD simulation

Figure 14 shows the predicted total RSI values of the entire roof assembly for roof assemblies with reflective air space thickness from 25 mm to 100 mm for clay tiles and concrete tiles. The total predicted RSI values are significantly higher for roof assemblies with roof pitch of 45° than roof assemblies with roof pitch 30°. Besides that, the total predicted RSI values increased as the thickness of the reflective air spaces increased from 25 mm to 100 mm, and the total RSI value for concrete tiles are consistently slightly lower than clay tiles for both roof pitches assembly. This is because clay tiles have lower thermal conductivity than concrete tiles. Hence, concrete tiles are able to transfer heat by heat conduction better than clay tiles which causes the heat flux penetration is slightly higher for roof assembly with concrete tiles. The CFD simulation predicts that the total RSI value passes the minimum RSI value as regulated in UBBL Section 38A-(2) when the reflective air space thickness is 50 mm and 60 mm for clay tiles and concrete tiles respectively for roof pitch of 30°. As for roof pitch of 45°, the RSI value passes the minimum regulated RSI value for all roof configurations.

Table 6 summarizes the predicted RSI values for all roof configuration of roof assemblies with roof pitch 30° and

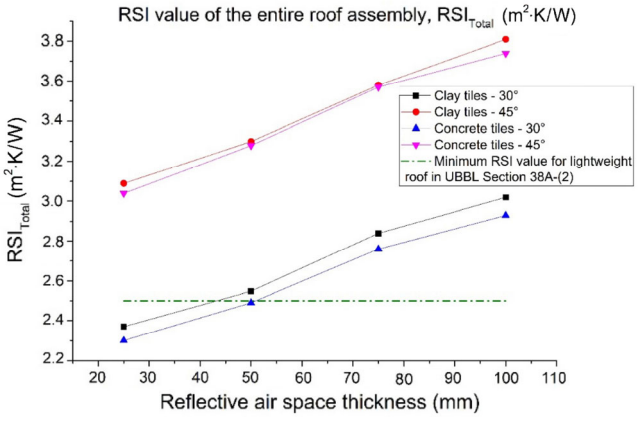

Fig. 14 The predicted total RSI value of the entire roof assembly

Table 6 Summary of all predicted RSI values (m^2·K/W)

Roof type	Roof Pitch	Reflective air space thickness											
		25 mm			50 mm			75 mm			100 mm		
		RSI_A	RSI_B	RSI_{Total}	RSI_A	RSI_B	RSI_{Total}	RSI_A	RSI_B	RSI_{Total}	RSI_A	RSI_B	RSI_{Total}
Clay tiles	30°	0.9	1.47	2.37	1.24	1.31	2.55	1.55	1.29	2.84	1.76	1.26	3.02
	45°	0.78	2.31	3.09	1.19	2.12	3.30	1.46	2.12	3.58	1.65	2.16	3.81
Concrete tiles	30°	0.83	1.5	2.33	1.2	1.32	2.52	1.5	1.26	2.76	1.69	1.24	2.93
	45°	0.72	2.32	3.04	1.17	2.11	3.28	1.43	2.14	3.57	1.63	2.11	3.74

roof pitch 45° using clay roof tiles and concrete roof tiles respectively.

From Table 6, it can be noted that:

(1) RSI_A for roof pitch of 45° are consistently slightly lower than roof pitch 30° for all reflective air space thicknesses.
(2) RSI_B for roof pitch of 45° are massively higher than roof pitch of 30° for all reflective air space thicknesses.
(3) While RSI_A increases as the thickness of reflective air space increases, the RSI_B decreases as the thickness reflective air space increases.

5 CFD graphical results

This section shows the CFD images obtained from the simulation. Note that the two parallel plates above the roof are the heat source directed towards the roof. This is to simulate heat radiation between 600 W/m^2 and 1000 W/m^2 to the roof.

5.1 CFD temperature cut plots of roof assemblies for a roof pitch of 30°

Figures 15 and 16 show the cut plots of temperature gradient in a 30° roof pitch assembly of without and with aluminum foil installed respectively. In Figure 16, the cut plot shows that there is a massive temperature reduction when an aluminum foil is installed. Majority amount of heat was trapped inside the reflective air space and reflected by the aluminum foil. Because of buoyancy force, the heat flows upwards and escapes through the ridge.

Comparing between Figures 16 and 17, there is a larger amount of heat that moves upwards towards the ridge

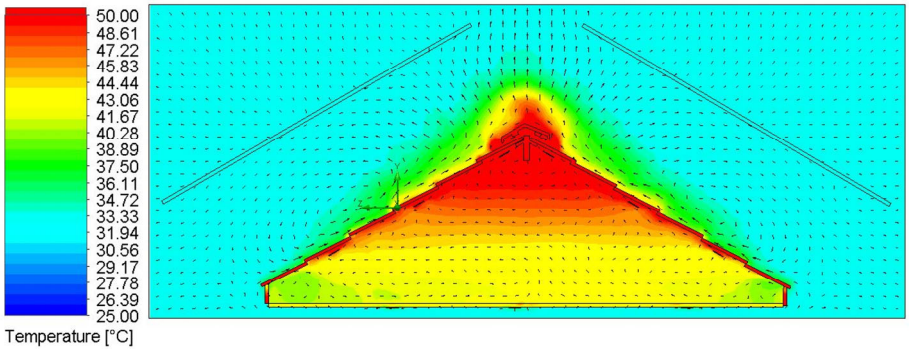

Fig. 15 Temperature gradient cut plot of 30° roof assembly without aluminum foil

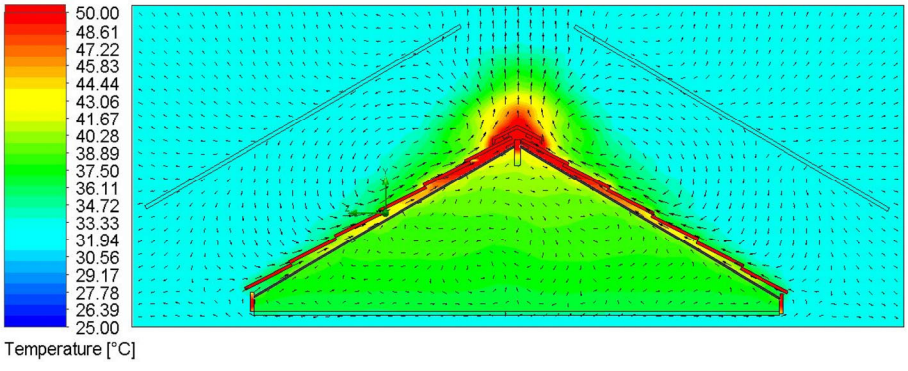

Fig. 16 Temperature gradient cut plot of 30° roof assembly with aluminum foil and reflective air space of 25 mm

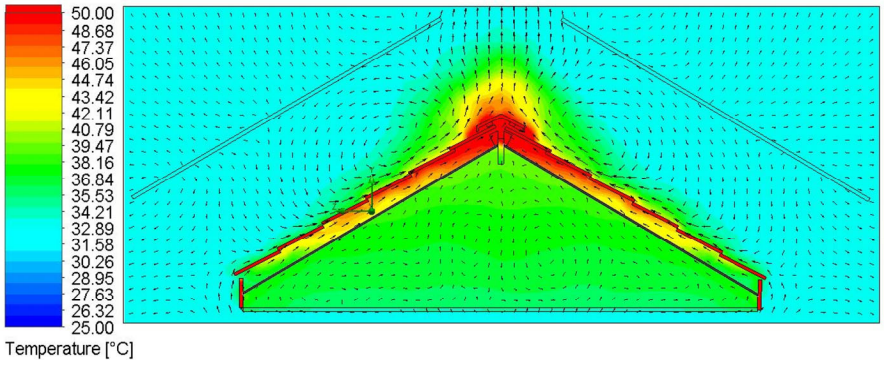

Fig. 17 Temperature gradient cut plot of 30° roof assembly with aluminum foil and reflective air space of 100 mm

when the thickness of the reflective air space is increased from 25 mm to 100 mm. Hence, lower heat penetration through reflective air space and the ceiling and this results in lower ceiling temperature when the thickness of reflective air space is increased from 25 mm to 100 mm.

5.2 CFD temperature cut plots of roof assemblies for a roof pitch of 45°

Figures 18 and 19 show the cut plots of temperature gradient in a 45° roof pitch assembly of without and with aluminum foil installed respectively. In Figure 18, the buoyancy effect has evidently taken place inside the attic space. Despite not having an aluminum foil installed, the hot air accumulates and escapes through the ridge due to buoyancy force. In Figure 19, the cut plot shows that the hot air was trapped and reflected by the aluminum foil in the reflective air space area. In the reflective air space area, the heat flows upwards from the eaves and escapes through the ridge.

Comparing between Figures 19 and 20, it can be seen that there is a larger amount of heat that moves upwards towards the ridge when the thickness of the reflective air space is increased from 25 mm to 100 mm. In the attic space, it is obvious that the air temperature is much lower when the reflective air space increases from 25 mm to 100 mm. Hence, when the thickness of the reflective air space is increased from 25 mm to 100 mm, heat penetration through the reflective air space and the attic space decrease. Furthermore, due to the escalated buoyance force in gable roof pitch of 45°, the hot air inside the attic moves upwards and escapes through the ridge and hence massively reduces the ceiling temperature.

6 Conclusions

The thermal performance of thermal insulated pitched roof assembly incorporating reflective insulation and radiant barrier systems was investigated in this paper. The study was performed by means of 3D CFD simulation with the aid of FloEFD. The predicted CFD results were validated against experimental measurement that was conducted by Teh et al. (2017)—a researcher from SERI UKM. The prediced CFD results were in good agreement with the empirical measurement with a ±95% confidence level, and a MAPE of 3.60%. The parameters investigated were the reflective air space thickness, roof pitch, and roof tile

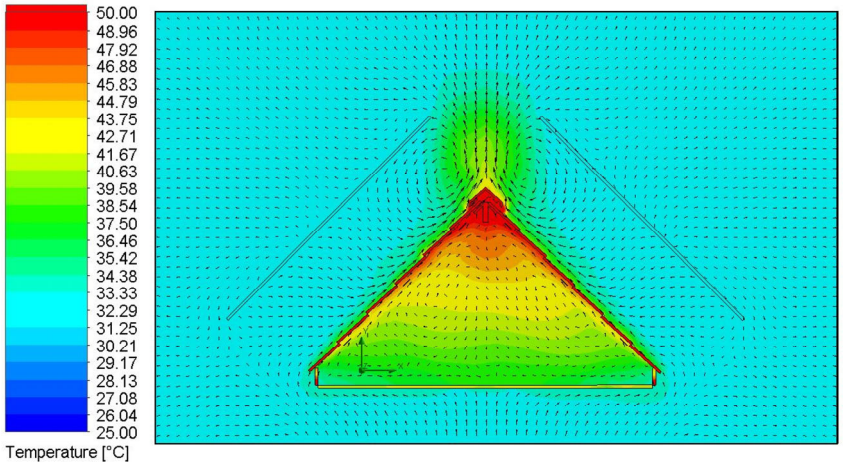

Fig. 18 Temperature gradient cut plot of 45° roof assembly without aluminum foil

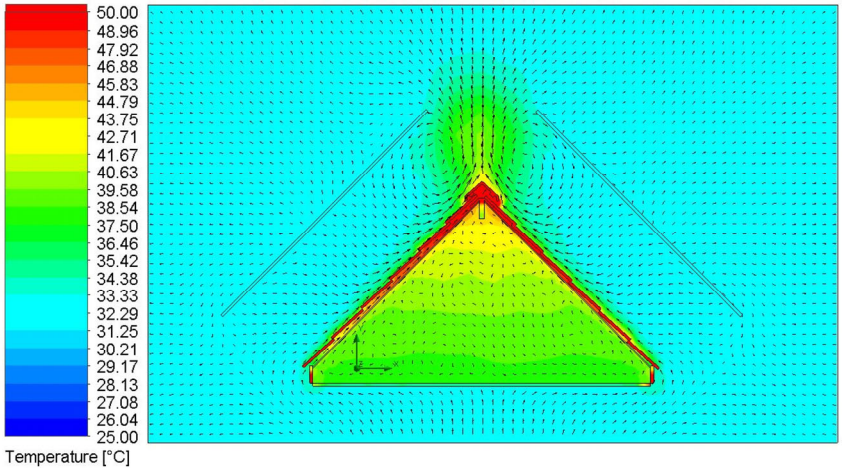

Fig. 19 Temperature gradient cut plot of 45° roof assembly with an insulation layer and 25 mm of air space

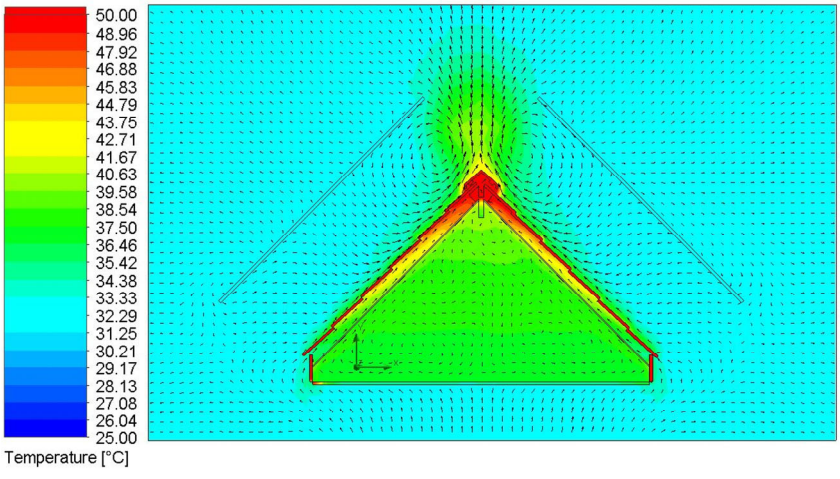

Fig. 20 Temperature gradient cut plot of 45° roof assembly with aluminum foil and reflective air space of 100 mm

material. The thermal performance of the thermal insulated gable roof assembly was by evaluating the reduction of heat flux across the roof assembly, and by calculating the RSI value of the roof assembly. The experimental measurement and CFD simulation results have led to the following conclusions:

- For roof pitch of 30°. the total predicted RSI value increases from 2.37 m^2·K/W and 2.33 m^2·K/W to 3.02 m^2·K/W and 2.93 m^2·K/W for clay tiles and concrete tiles respectively, with increasing the reflective air space thickness from 25 mm to 100 mm. For roof pitch of 45°, the total predicted RSI value increases from 3.09 m^2·K/W and 3.04 m^2·K/W to 3.81 m^2·K/W and 3.74 m^2·K/W for clay tiles and concrete tiles respectively, with increasing the reflective air space thickness from 25 mm to 100 mm. As the thickness of reflective air space increases from 25 mm to 100 mm, the decrease of heat gain increases from 79% to 88% and 84% to 87% for roof pitch of 30° and 45° respectively.
- Heat flux penetration through the reflective air space decreases as the thickness of reflective air space thickness increases from 25 mm to 100 mm as air flows from the eaves of the roof and escapes through the ridge.
- The RSI value of roof assembly with a roof pitch of 45° is significantly higher than roof assembly with a roof pitch of 30°. As the roof pitch is increased from 30° to 45°, the buoyancy effect increases in the attic space and reduces heat accumulation which results in lower heat flux penetration.
- The results also showed that there is only a slight difference in thermal resistivity of the roof assembly between clay tiles and concrete tiles. The overall behavior of heat transfer across the roof assembly was the same between the two materials of roof tiles.
- The CFD simulation predicts that roof pitch of 30°, the total RSI value passes the minimum RSI value of 2.5 m^2/W·K when the reflective air space thickness is 50 mm and 60 mm for clay tiles and concrete tiles respectively for roof pitch of 30°. As for roof pitch of 45°, the RSI value passes the minimum regulated RSI value for all roof configurations.

The research demonstrates that the application of reflective insulation and radiant barrier systems in a gable roof is able to provide an adequate amount of thermal insulation for a building. The parametric studies showed that varying the roof pitch has first-order impact on reducing heat flux penetration through the attic space, followed by varying the reflective air space thickness and roof materials. The degree of improvement in terms of indoor thermal comfort that the thermal insulation systems are able to provide will be the focus of future researches. Finally, the use of CFD method provides an alternative method in investigation thermal insulation technology in buildings and this method should be explored further.

Acknowledgements

The authors would like to thank the National University of Malaysia (UKM) for their financial support under the grant AP-2017-006/1 and AP-2017-006/4.

References

Alzwayi AS, Paul MC (2014). Transition of free convection flow inside an inclined parallel walled channel: Effects of inclination angle and width of the chan nel. *International Journal of Heat and Mass Transfer*, 68: 194–202.

Department of Standards Malaysia (2014). Energy Efficiency and Use of Renewable Energy for Residential Buildings—Code of Practice (MS 1525:2014).

Dimoudi A, Androutsopoulos A, Lykoudis S (2006). Summer performance of a ventilated roof component. *Energy and Buildings*, 38: 610–617.

Fantucci S, Serra V (2019). Investigating the performance of reflective insulation and low emissivity paints for the energy retrofit of roof attics. *Energy and Buildings*, 182: 300–310.

Gagliano A, Patania F, Nocera F, Ferlito A, Galesi A (2012). Thermal performance of ventilated roofs during summer period. *Energy and Buildings*, 49: 611–618.

Hernández-Pérez I, Álvarez G, Xamán J, Zavala-Guillén I, Arce J, Simá E (2014). Thermal performance of reflective materials applied to exterior building components—A review. *Energy and Buildings*, 80: 81–105.

Lee SW, Lim CH, Salleh EIB (2016). Reflective thermal insulation systems in building: a review on radiant barrier and reflective insulation. *Renewable and Sustainable Energy Reviews*, 65: 643–661.

Lee S, Park SH, Yeo MS, Kim KW (2009). An experimental study on airflow in the cavity of a ventilated roof. *Building and Environment*, 44: 1431–1439.

Li D, Zheng Y, Liu C, Qi H, Liu X (2016). Numerical analysis on thermal performance of naturally ventilated roofs with different influencing parameters. *Sustainable Cities and Society*, 22: 86–93.

Medina MA (2000). On the performance of radiant barriers in combination with different attic insulation levels. *Energy and Buildings*, 33: 31–40.

Medina MA (2012). A comprehensive review of radiant barrier research including laboratory and field experiments. *ASHRAE Transactions*, 118 (1): 400–407.

Medina MA, Young B (2006). A perspective on the effect of climate and local environmental variables on the performance of attic radiant barriers in the United States. *Building and Environment*, 41: 1767–1778.

Mentor Graphics Cooperation (2017). FloEFD Technical Reference Version 17. Avaiable at https://www.mentor.com.

Miranville F, Fakra AH, Guichard S, Boyer H, Praene JP, Bigot D (2012). Evaluation of the thermal resistance of a roof-mounted multi-reflective radiant barrier for tropical and humid conditions: Experimental study from field measurements. *Energy and Buildings*, 48: 79–90.

Nahar NM, Sharma P, Purohit MM (2003). Performance of different passive techniques for cooling of buildings in arid regions. *Building and Environment*, 38: 109–116.

RIMA (2002). Reflective Insulation , Radiant Barriers And Radiation Control Coatings, 2nd Edition.

Roels S, Deurinck M (2011). The effect of a reflective underlay on the global thermal behaviour of pitched roofs. *Building and Environment*, 46: 134–143.

Saber HH (2013). Thermal performance of wall assemblies with low emissivity. *Journal of Building Physics*, 36: 308–329.

dos Santos GH, Mendes N (2015). Numerical analysis of hygrothermal performance of reflective insulated roof coatings. *Applied Thermal Engineering*, 81: 66–73.

Sarawak Energy (2017). Solar Energy by Sarawak Energy. Sarawak Energy. Available at https://www.sarawakenergy.com/what-we-do/power-generation.

Soubdhan T, Feuillard T, Bade F (2005). Experimental evaluation of insulation material in roofing system under tropical climate. *Solar Energy*, 79: 311–320.

Teh KS, Yarbrough DW, Lim CH, Salleh E (2017). Field evaluation of reflective insulation in South East Asia. *Open Engineering*, 7 (1): 352–362. https://doi.org/10.1515/eng-2017-0039.

Tong S, Li H (2014). An efficient model development and experimental study for the heat transfer in naturally ventilated inclined roofs. *Building and Environment*, 81: 296–308.

Troppová E, Tippner J, Švehlík M (2018). Numerical and experimental study of conjugate heat transfer in a horizontal air cavity. *Building Simulation*, 11: 339–346.

Wang S, Shen Z, Gu L (2012). The impact of roof pitch and ceiling insulation on cooling load of naturally-ventilated attics. *Energies*, 5: 2178–2196.

Yarbrough DW (2010). Reflective materials and radiant barriers for insulation in buildings. In: Hall MR, Materials for Energy Efficiency and Thermal Comfort in Buildings. Cambridge, UK: Woodhead Publishing. pp. 305–318.

Yarbrough DW, Teh KS, Lim CH, Salleh E, Mat S, Sulaiman MY (2016). Hybrid and reflective insulation assemblies for buildings. *Journal of Power and Energy Engineering*, 4: 23–31.